

CMS results on top spin correlations and entanglement

Regina Demina^{a,*}

^aUniversity of Rochester,

500 Wilson blvd, Rochester, NY, USA

E-mail: regina@pas.rochester.edu

Quantum entanglement of top and antitop quarks based on the spin degrees of freedom has been demonstrated using LHC data collected by the CMS experiment in the period of 2016-2018. Top quark decays to a bottom quark and a W boson, which decays either leptonically or to a quark-antiquark pair. Pair production of top quarks with both W bosons decaying leptonically is referred to as a dilepton channel, since it contains two charged leptons. The channel containing one of the W bosons decaying into a quark-antiquark pair, is referred to as a lepton+jets channel. We present the results in both channel. Using the opening angle between the two charged leptons, an entanglement has been demonstrated at the threshold of the top pair production in the dilepton channel. Using lepton+jets channel we perform a measurement of the top and antitop quark polarization and spin correlation in bins of the invariant mass of the system and the top quark scattering angle. Using the spin correlation matrix we demonstrate the entanglement at the production threshold and at the high invariant mass.

12th Large Hadron Collider Physics Conference (LHCP2024)
3-7 June 2024
Boston, USA

*Speaker

The top and antitop quarks are spin $1/2$ particles, which present the most elementary units of quantum information - qubits. At the LHC top quarks are produced in a single reaction, typically gluon-gluon fusion, which implies that the top and antitop quarks were interacting with each other at some point in time. They therefore form a two qubit system, whose state can be either separable or entangled. Top quark decays predominantly to a bottom quark, which hadronizes into a b-jet, i.e a jet containing a B hadron, and a W boson, which can decay either to a charged lepton and a neutrino, or a pair of light quarks. Thus, top pair production is characterized by the presence of two b-jets, and either a charged lepton and two lighter jets, or a pair of charged leptons. The former case is referred to as a lepton+jets channel, while the later as a dilepton channel. The correlation of the spin orientations \vec{s}/\vec{s}' of top/antitop quarks is described by the spin correlation matrix C_{ij} , where $i, j = 1, 2, 3$ are the 3D coordinates of the spin vectors. Top quark is a short-lived particle with a lifetime of order 10^{-25} s. W boson decay products are long-lived and hence are ideal probes of the spin correlation.

The experimentally observable directions of motion of W boson decay products p/p' , described by the unit vectors $\vec{\Omega}_{p/p'} = (\sin \theta_{p/p'} \cos \phi_{p/p'}, \sin \theta_{p/p'} \sin \phi_{p/p'}, \cos \theta_{p/p'})$, are correlated with the top quarks' spin orientation, and as such can be used as statistical measures of the spin correlation. The differential cross section is given by

$$\frac{d\sigma}{d\Omega_p d\Omega_{p'}} = \sigma_{\text{norm}}(1 + \kappa_p \vec{P} \vec{\Omega}_p + \kappa_{p'} \vec{P}' \vec{\Omega}_{p'} - \kappa_p \kappa_{p'} \vec{\Omega}_p C \vec{\Omega}_{p'}), \quad (1)$$

where $\kappa_p/\kappa_{p'}$ are the spin analyzing powers of p/p' . Their values are maximal for charged leptons and d -type (d or s) quarks. \vec{P}/\vec{P}' are the top/antitop quark polarization vectors. Assuming that \vec{P}/\vec{P}' and C are not known, the cross section linearly depends on $15 = 3 + 3 + 9$ free parameters. The overall normalization, σ_{norm} , adds one more parameter. Let us refer to these parameters collectively as Q_m , $m = 0, \dots, 15$. CMS developed an approach that allows to experimentally evaluate all these 16 parameters, and applied this method to CMS Run 2 data [2].

In quantum mechanics a system is considered separable if its density matrix can be factored into that of individual states, otherwise it is considered entangled. According to the Peres-Horodecki criterion [3, 4], constructed using diagonal elements of C_{ij} in the helicity basis $\{k, r, n\}$ [5], the system is entangled if

$$\Delta_E = C_{nn} + |C_{rr} + C_{kk}| > 1. \quad (2)$$

Thus, based on the values of C_{ij} it is possible to determine if the system of top and anti top quarks is in an entangled state. Alternatively, without measuring the full matrix C it is still possible to evaluate the Perez-Horodecki criterion based on the opening angle χ between the two top decay products p and p' . The cross section dependence on χ is given by:

$$\frac{d\sigma}{d \cos \chi} = \sigma_{\text{norm}}(1 + \kappa_p \kappa_{p'} D \cos \chi), \quad (3)$$

If $C_{ii} > 0$, which is expected to be the case at the threshold of $t\bar{t}$ production, where top and anti top quarks form a singlet state, the Perez-Horodecki criterion takes the form

$$C_{nn} + C_{rr} + C_{kk} = \text{tr}(C) = -3D > 1. \quad (4)$$

For high values of the invariant mass of the $t\bar{t}$ system, $M_{t\bar{t}}$, where the top and anti top quarks are in the triplet state, the coefficients C_{rr} and C_{kk} are negative. In this case the angle $\tilde{\chi}$ is defined such that the sign of the n -component in one of the decay products is inverted. Then, the condition for entanglement has a form

$$C_{nn} - C_{rr} - C_{kk} = -3\tilde{D} > 1. \quad (5)$$

We present the results in the lepton+jets and in the dilepton channels using the full evaluation of the spin correlation matrix, and the measurements of coefficient D and \tilde{D} . The two channels have different strength and weaknesses. The dilepton channel, though having a lower branching ratio is cleaner. Easy to identify leptons have lower minimum transverse momentum compared to jets. This is particularly advantageous at the threshold of the $t\bar{t}$ production. At the same time the precision in the determination of $M_{t\bar{t}}$ in the dilepton channel is complicated by the presence of two unregistered neutrinos. Based on these considerations dilepton channel has an advance at the threshold of the $t\bar{t}$ production, while lepton+jets channel has an edge at the high $M_{t\bar{t}}$, where the statistics is limited.

Accurate modeling of the top pair production is very important in this analysis. We use $t\bar{t}$ samples produced using NLO QCD Monte Carlo generator POWHEG [6], coupled with Pythia 8 [7] to model the hadronization process, which was tuned on CMS data [8]. On top of that we apply the correction due to electroweak processes evaluated using HATHOR [10]. We also modify the kinematic distributions to account for the NNLO QCD effects [9]. There is a possibility for a production of the $t\bar{t}$ bound state, a.k.a toponium, just below the threshold of the $t\bar{t}$ production. This can affect both the $M_{t\bar{t}}$ distribution and the level of spin correlation in the $t\bar{t}$ system. We include modeling of the toponium production using a parametrized model put forward in [11].

We present the modeled distribution in the opening angle between the two charged leptons in the dilepton system in Fig. 1 (left). Different colors represent different levels of the spin correlation varied from -100 to +100%. By comparing the expected and observed distributions in the opening angle (as shown in Fig. 1 (center)) we are able to determine the value of the coefficient D in Eq. 3. The measured value is shown in Fig. 1 (right) for the two cases - one where toponium is included in the model and one where it is not included. Both observed and predicted values are affected by this assumption. We see that there is a better agreement between the observation and the prediction in the case where toponium is included in the model, while the statistical precision is not sufficient to completely exclude either of the hypotheses.

Identification of charged leptons, in particular electrons and muons is easy, while deciding which of the light jets originate from the d -type quark presents a significant challenge. Since the W boson decays via a weak interaction, it imprints a certain pattern on the kinematics of its decay products. In particular, d -type quarks tend to move in the direction opposite to W boson momentum. In 50% of the W boson decays one of the jets is associated with a charm quark, which is a u -type quark, hence the other jet must be of a d -type. Charm jets tend to contain tracks displaced from the primary vertex due to a fairly long lifetime of the charm quark. The information about the kinematics and the displacement of the tracks is fed into a neural net, which optimizes the assignment of the observed objects - jets and leptons - to the decays products of top and antitop quarks. The distribution in the neural net score is shown in Fig. 2(left). Depending on the event category the efficiency of the fully correct assignment can be as high as 65%, as shown in

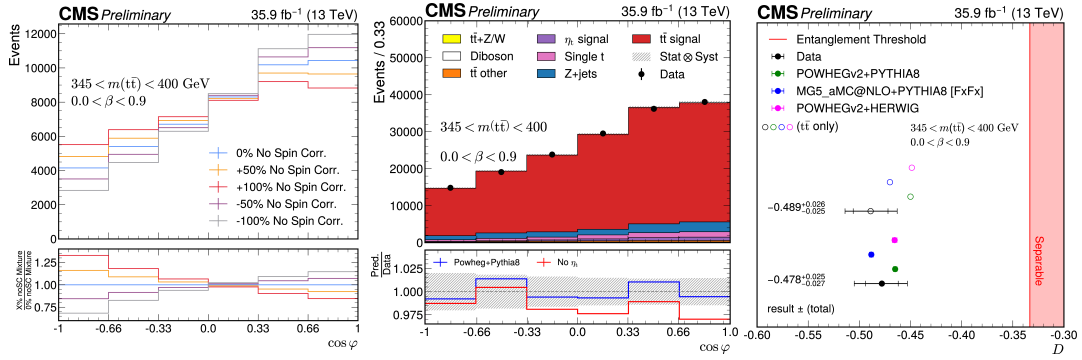


Figure 1: Figures from [1]. Left: Distribution over the opening angle between the two charged leptons for different levels of spin correlation (legend inline). Center: fit to the data. Right: The value of D in the dilepton channel.

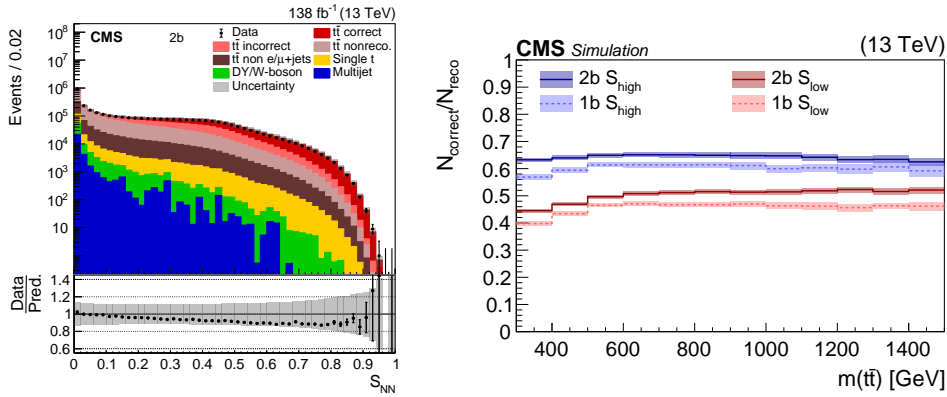


Figure 2: Figures from [2]. Left: Distribution of S_{NN} for the events containing two identified b jets. The data (points) are compared to the prediction (stacked histograms). The $t\bar{t}$ contribution is split into the correctly and incorrectly reconstructed, “nonreconstructable”, and non e/μ +jets events. The gray uncertainty band indicates the combined statistical and systematic uncertainties in the prediction, while the vertical bars on the points show the statistical uncertainty of the data. The ratios of data to the predicted yields are provided in the lower panels. Right: Reconstruction efficiency as a function of $M_{t\bar{t}}$ estimated from the simulation. The values are shown separately for the events containing one identified b -jet ($1b$) and two ($2b$) and divided by NN score low ($S_{NN} < 0.36$) and high ($S_{NN} > 0.36$) categories.

Fig. 2(right).

The observed angular distribution of p/p' can be described by a linear combination of functions Σ_m with coefficients Q_m . The dependence of Σ_m on the angles of the decay products can be read from Eq. 1:

$$\Sigma_m = (1, \kappa_p \sin \theta_p \cos \phi_p, \dots, \kappa_{p'} \cos \theta_{p'}, -\kappa_p \kappa_{p'} \sin \theta_p \cos \phi_p \sin \theta_{p'} \cos \phi_{p'}, \dots, -\kappa_p \kappa_{p'} \cos \theta_p \cos \theta_{p'}), \quad (6)$$

and are shown in red in Fig. 3(left). Yet, once the detector effects, such as selection efficiency, are taken into account, these functions are modified as shown in blue in Fig. 3 (left). The templates defined at the detector level are used to fit for the data distribution in the angular variables to extract

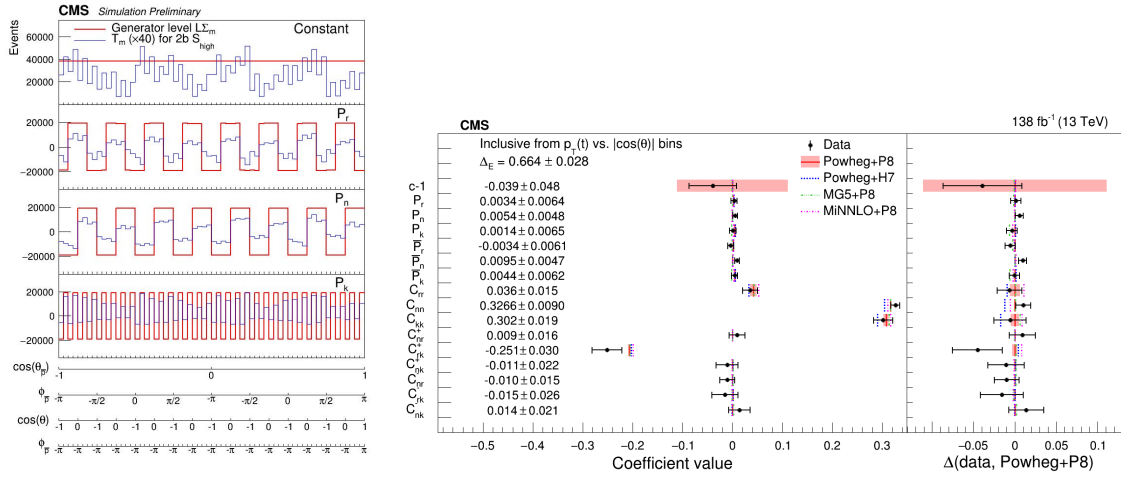


Figure 3: Figures from [2]. Examples of angular templates Σ_m at the generator level (red) and at the detector level (blue). In this figure the angles describing the direction of the decay products p/p' are rolled out into 1D 64 bin variable as shown in the bottom panels. Right: Result of the fit to data. The extracted components of the polarization vectors and spin correlation matrix are compared to the prediction based on different simulations listed inline.

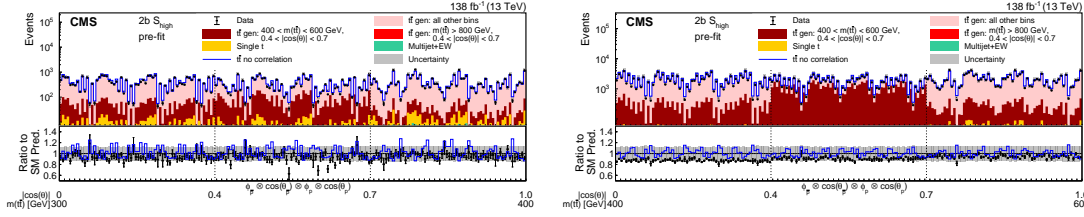


Figure 4: Figures from [2]. Pre (left) and post (right) fit distributions comparing the data (points) to the POWHEG + PYTHIA simulation (stacked histograms) for the full matrix measurement in bins of $M_{t\bar{t}}$ vs. $|\cos(\theta)|$ in the $2b S_{high}$ category. The x axis shows the bins of the unrolled 4-dimensional distribution of the angles, listed from the outermost to the innermost variable in each of the $M_{t\bar{t}}$ vs. $|\cos(\theta)|$ bins. The boundaries of the $|\cos(\theta)|$ and $M_{t\bar{t}}$ bins are labeled and indicated by dashed and solid lines, respectively. All other $t\bar{t}$ contributions are shown in pink, the ones corresponding to the $M_{t\bar{t}}$ bin at the generator level - in red. A model without any polarization and spin correlation is shown as a blue line. The gray uncertainty band indicates the combined statistical and systematic uncertainties in the prediction. The vertical bars on the points show the statistical uncertainty. Ratios to the predicted yields are provided in the lower panels.

the values of Q_m . An example of the pre- and post-fit distributions is shown in Fig. 4. The result of such a fit is shown in Fig. 3 (right), where the measured values of the polarization vectors and spin correlation matrix are shown to be in a good agreement with the prediction of the simulation based on the Standard Model.

Based on the measured values of the spin correlation matrix the Δ_E criterion is evaluated and shown in Fig. 5. The observed value of Δ_E exceed the threshold value of 1 by more than 6 standard deviations in the high invariant mass region (left plot), thus passing Peres-Horodecki criterion. Hence, the system is considered entangled in this region of phase space. To ensure that the observed

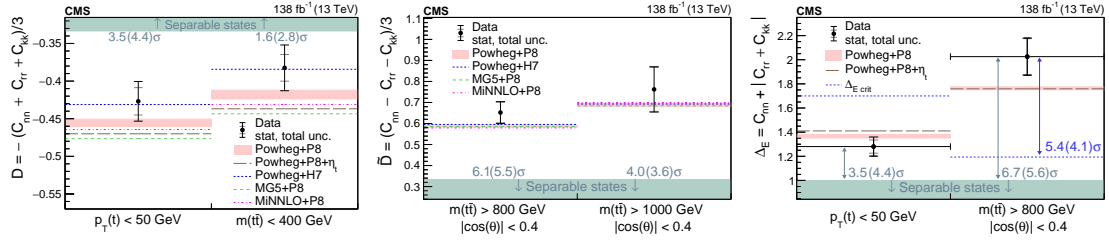


Figure 5: Figures from [2]. Entanglement results for the D measurement in the threshold region (left), \bar{D} measurement in the high- $M_{t\bar{t}}$ region (center), and the full matrix measurement in different $M_{t\bar{t}}$ regions (lower). The measurements (points) are shown with the statistical uncertainty (inner error bars) and total uncertainty (outer error bars) and compared to the predictions of different models (legend inline). The POWHEG + PYTHIA prediction is displayed with the ME scale and PDF uncertainties, while for all other predictions only the central values are indicated. The observed (expected) significance of the deviation from the boundary of separable states (green region) is quoted in standard deviations (σ). Right: The horizontal blue lines correspond to the maximum level of entanglement ΔE_{crit} that can be explained by the exchange of information between top and anti top at the speed of light. The significance in standard deviations (σ) by which the measurement exceeds ΔE_{crit} and unity is quoted in blue and light green, respectively, and indicated by the corresponding arrows.

level of entanglement cannot be explain by classical communication we follow citeDemina2024 and introduce ΔE_{crit} . This parameter is set to maximally allowed value of 3 for the events where the $t\bar{t}$ pairs are in causal contact with other, and to 1, which is the maximally allowed value for separable state, for the rest of the events. As demonstrated in Fig. 5 (right) the observed value of Δ_E exceeds ΔE_{crit} (shown by dashed blue line) by more than 5 standard deviations.

Using dilepton events CMS demonstrated that $t\bar{t}$ pairs are produced in an entangled state at the threshold of the production. Using lepton+jets events it was also shown that entangled state is also produced at the high values of the invariant mass, where it cannot be explain by the classical exchange of information.

References

- [1] A. Hayrapetyan and others, *Observation of quantum entanglement in top quark pair production in proton–proton collisions at $\sqrt{s} = 13$ TeV*, *Rept. Prog. Phys.*, **87**, (2024), 117801.
- [2] A. Hayrapetyan and others, *Measurements of polarization, spin correlations, and entanglement in top quark pairs using lepton+jets events from pp collisions at $\sqrt{s} = 13$ TeV*, accepted by PRD.
- [3] A. Peres, *Separability Criterion for Density Matrices*, *Phys. Rev. Lett.*, **77** (1996)1413.
- [4] M. Horodecki, P. Horodecki, R. Horodecki, *Separability of mixed states: necessary and sufficient conditions*, *Physics Letters A*, **223** (1996) 1.
- [5] W. Bernreuther, Z.-G. Si *Top quark spin correlations and polarization at the LHC: standard model predictions and effects of anomalous top chromo moments*, *Phys. Lett. B*, **725** (2013)115.

- [6] *A general framework for implementing NLO calculations in shower Monte Carlo programs: the POWHEG BOX*, *JHEP*, **06** (2010) 043.
- [7] T.Sjostrand et al., *An introduction to PYTHIA8.2*, *Comput.Phys.Commun.*, 191, **38** (2015) 717718.
- [8] CMS Collaboration, *Extraction and validation of a new set of CMS PYTHIA8 tunes from underlying-event measurements*, *Eur. Phys. J. C*, **80** (2020) 4.
- [9] J. Mazzitelli et al., *Next-to-Next-to-Leading Order Event Generation for Top-Quark Pair Production*, *Phys. Rev. Lett.*, **127** (2021) 062001.
- [10] M. Aliev et al., *HATHOR: HAdronic Top and Heavy quarks cross section calculator*, *Comput. Phys. Commun.*, **182** (2011) 1034.
- [11] B. Fuks et al. *Phys. Rev. D*, **104** (2021) 034023.
- [12] R. Demina, G. Landi *Locality in collider tests of Quantum Mechanics with top quark pairs* 2407.15223v1(2024).